FUNCTIONAL NEURORADIOLOGY

Diffusion tensor mode in imaging of intracranial epidermoid cysts: one step ahead of fractional anisotropy

**Milan Jolapara · Chandrasekharan Kesavadas ·
V. V. Radhakrishnan · Jitender Saini ·
Satya Narayan Patro · Arun Kumar Gupta ·
Tirur Raman Kapilamoorthy · Narendra Bodhey**

Abstract

Introduction The signal characteristics of an epidermoid on T2-weighted imaging have been attributed to the presence of increased water content within the tumor. In this study, we explore the utility of diffusion tensor imaging (DTI) and diffusion tensor metrics (DTM) in knowing the microstructural anatomy of epidermoid cysts.

Materials and methods DTI was performed in ten patients with epidermoid cysts. Directionally averaged mean diffusivity (D_{av}), exponential diffusion, and DTM-like fractional anisotropy (FA), diffusion tensor mode (mode), linear (CL), planar (CP), and spherical (CS) anisotropy were measured from the tumor as well as from the normal-looking white matter.

Results Epidermoid cysts showed high FA. However, D_{av} and exponential diffusion values did not show any restriction of diffusion. Diffusion tensor mode values were near −1, and CP values were high within the tumor. This suggested preferential diffusion of water molecules along a two-dimensional geometry (plane) in epidermoid cysts, which could be attributed to the parallel-layered arrangement of keratin filaments and flakes within these tumors.

Conclusion Thus, advanced imaging modalities like DTI with DTM can provide information regarding the microstructural anatomy of the epidermoid cysts.

Keywords Epidermoid · DTI · Fractional anisotropy · Diffusion tensor mode · Pathology

Introduction

Epidermoid cysts are relatively rare intracranial neoplasms. They present mostly as extra-axial tumors; however, they may also present as intraventricular mass lesions [1, 2]. The hyperintensity in the diffusion-weighted imaging (DWI) is a characteristic finding in these tumors. This finding helps to diagnose this tumor even when they are placed at unusual locations. The reasons for these signal changes in diffusion have been debated in the literature [3–5]. Diffusion tensor imaging (DTI) has been used to study the microstructure of brain lesions [6]. Understanding the various diffusion tensor metrics can give an idea about the arrangement of cells/fibers within a neoplasm [7–10]. Our study has analyzed the various metrics in epidermoid cyst so as to understand the diffusion characteristics within this tumor.

Materials and methods

Ten patients with pathologically proven epidermoid cysts were included in this retrospective study. Magnetic resonance (MR) examination of the brain was performed on a 1.5-T clinical MR Scanner (Avanto TIM SQ engine; Siemens, Erlangen, Germany) in all the patients. Each patient underwent conventional magnetic resonance imaging

M. Jolapara · C. Kesavadas (✉) · J. Saini · S. N. Patro ·
A. K. Gupta · T. R. Kapilamoorthy · N. Bodhey
Department of Imaging Sciences and Interventional Radiology,
Sree Chitra Tirunal Institute for Medical Sciences
and Technology,
Trivandrum 695011, India
e-mail: chandkesav@yahoo.com

V. V. Radhakrishnan
Department of Pathology, Sree Chitra Tirunal Institute for Medical
Sciences and Technology,
Trivandrum 695011, India

Table 1 Summary of D_{av}, exponential diffusion (EXP) and DTI metrics (FA, Mode, CL, CP, and CS) measured from epidermoid cysts and normal white matter of posterior limb of internal capsule and splenium of corpus callosum.

		Cases											Mean
		Case 1	Case 2	Case 3	Case 4	Case 5	Case 6	Case 7	Case 8	Case 9	Case 10	
Age (in years)		30	44	4	35	45	52	45	35	65	25	
DTI metrics	Lesion											
	D_{av}	0.766	0.82	1.366	0.65	0.857	0.758	1.129	1.006	0.822	0.917	0.909
	EXP	0.466	0.441	0.255	0.524	0.425	0.469	0.324	0.37	0.44	0.399	0.411
	FA	0.467	0.631	0.309	0.554	0.441	0.439	0.56	0.38	0.428	0.463	0.467
	Mode	−0.934	−0.97	−0.722	−0.965	−0.942	−0.847	−0.951	−0.96	−0.942	−0.974	−0.921
	Linear	0.039	0.037	0.048	0.034	0.033	0.052	0.038	0.021	0.027	0.023	0.035
	Planar	0.542	0.811	0.309	0.676	0.511	0.484	0.687	0.44	0.499	0.553	0.551
	Spherical	0.42	0.152	0.643	0.29	0.456	0.463	0.275	0.538	0.474	0.425	0.414
	Posterior limb of internal capsule											
	D_{av}	0.725	0.676	0.786	0.713	0.789	0.718	0.784	0.687	0.795	0.694	0.737
	EXP	0.486	0.51	0.456	0.492	0.456	0.495	0.459	0.503	0.453	0.5	0.481
	FA	0.821	0.79	0.781	0.776	0.726	0.801	0.787	0.752	0.778	0.874	0.789
	Mode	0.937	0.903	0.971	0.952	0.86	0.934	0.864	0.854	0.846	0.943	0.906
	Linear	0.598	0.567	0.57	0.548	0.461	0.59	0.534	0.49	0.514	0.705	0.558
	Planar	0.161	0.165	0.93	0.137	0.212	0.105	0.237	0.207	0.244	0.135	0.253
	Spherical	0.242	0.268	0.338	0.315	0.327	0.305	0.228	0.302	0.242	0.16	0.273
	Splenium of corpus callosum											
	D_{av}	0.837	0.781	0.822	0.855	0.784	0.861	0.599	0.77	0.712	0.722	0.774
	EXP	0.434	0.459	0.441	0.426	0.46	0.425	0.551	0.464	0.494	0.487	0.464
	FA	0.82	0.839	0.894	0.761	0.835	0.803	0.857	0.849	0.79	0.865	0.831
	Mode	0.946	0.986	0.975	0.95	0.967	0.929	0.977	0.989	0.944	0.981	0.964
	Linear	0.599	0.665	0.725	0.529	0.634	0.682	0.668	0.679	0.564	0.686	0.643
	Planar	0.149	0.7	0.121	0.126	0.132	0.124	0.109	0.079	0.146	0.103	0.179
	Spherical	0.251	0.265	0.154	0.345	0.234	0.193	0.223	0.242	0.291	0.212	0.241

Values represent mean, and the unit of D_{av} is $\times 10^{-3}$ s/mm^2. FA and other DTI metrics are dimensionless
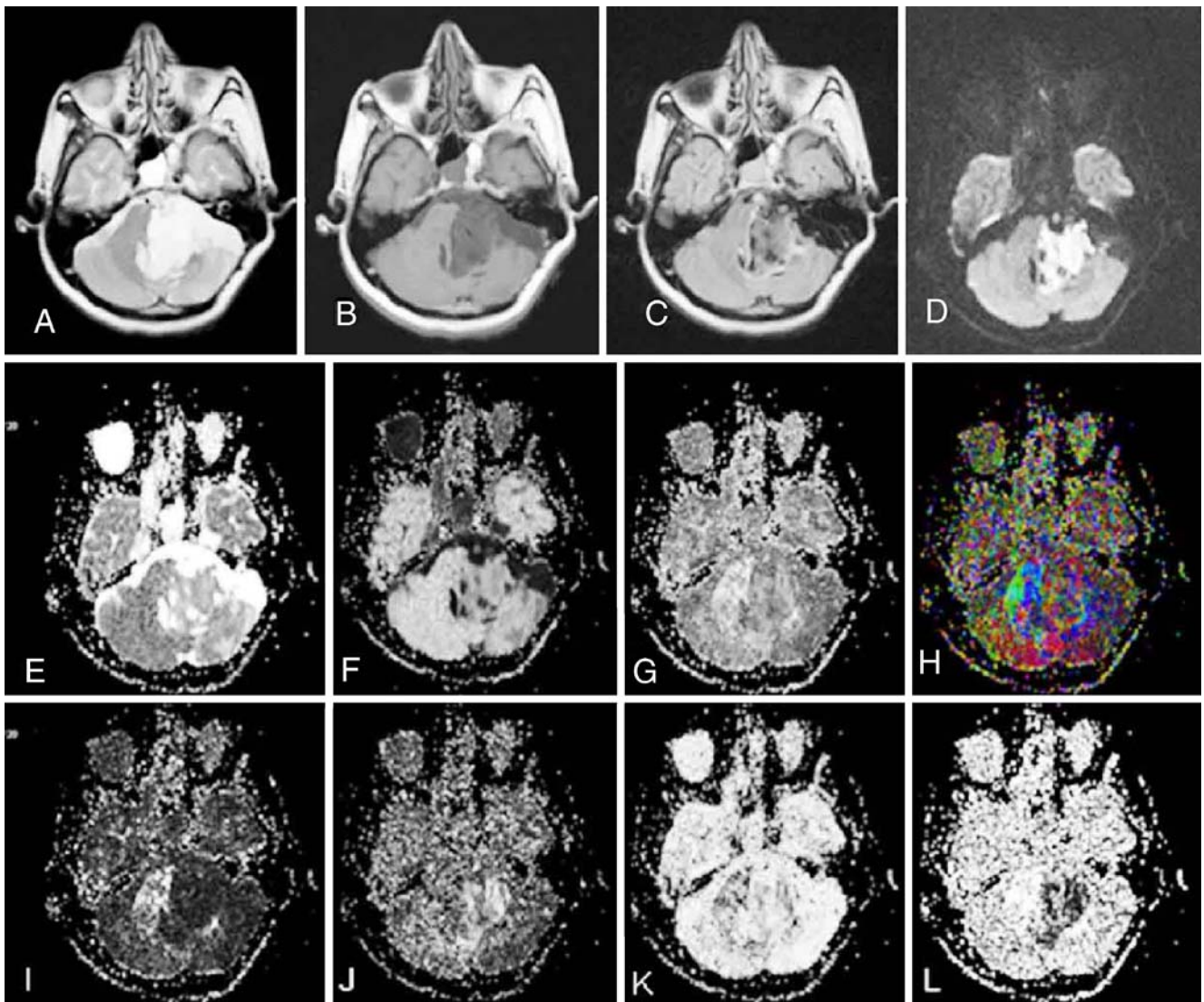
Fig. 1 Case 7: Axial T2-weighted image (**A**) shows hyperintense epidermoid cyst in the left cerebello-pontine angle. It appears hypointense on T1-weighted image (**B**) and heterogeneous on axial FLAIR image (**C**). On diffusion trace image (**D**) the lesion appears bright, while on apparent diffusion coefficient map (**E**) it appears isointense to hyperintense and on exponential diffusion image (**F**) it appears isointense to hypointense. FA (**G**) and directionally color-encoded FA (**H**) maps show high FA inside the tumor. High signal intensity seen in the CP (**J**) map and low signal intensity on diffusion tensor mode (**L**) and CL (**I**) maps suggest that increased FA is due to preferential diffusion occurring along a plane. Low signal intensity on CS (**K**) map suggests decrease in isotropic diffusion

with T1, T2, and fluid-attenuated inversion recovery (FLAIR) sequences. Then, a spin-echo echo-planar DTI sequence was performed with diffusion gradients along 30 non-collinear directions with the following imaging parameters: TR 3,500 ms, TE 105 ms, matrix 192×192, field of view (FOV) 230 mm^2, 5 mm slice thickness with 1.5 mm gap, averaged twice and with a b factor of 0 and 1,000 s/mm^2.

The DTI study analysis was performed by two neuroradiologists (MJ and CK). The analysis and postprocessing were performed on a separate workstation (Leonardo, Siemens, Erlangen, Germany). The regions of interest (ROI) were placed within the solid-appearing portions of the tumor appearing hyperintense on planar anisotropy maps and hypointense on diffusion tensor mode maps. Also, for comparison, the ROI were placed in the normal white matter regions (posterior limb of internal capsule and splenium of corpus callosum). The size of the ROI (6 pixels) was kept constant in all the cases and at all the regions. While placing the ROI, proper care was taken to avoid partial volume effects from adjacent brain parenchyma and cerebrospinal fluid. The D_{av} and exponential diffusion were calculated. Diffusion tensor metrics (DTM) including fractional anisotropy (FA), linear (CL), planar (CP), and spherical (CS) anisotropy and diffusion tensor mode were computed using the software provided by the vendor.
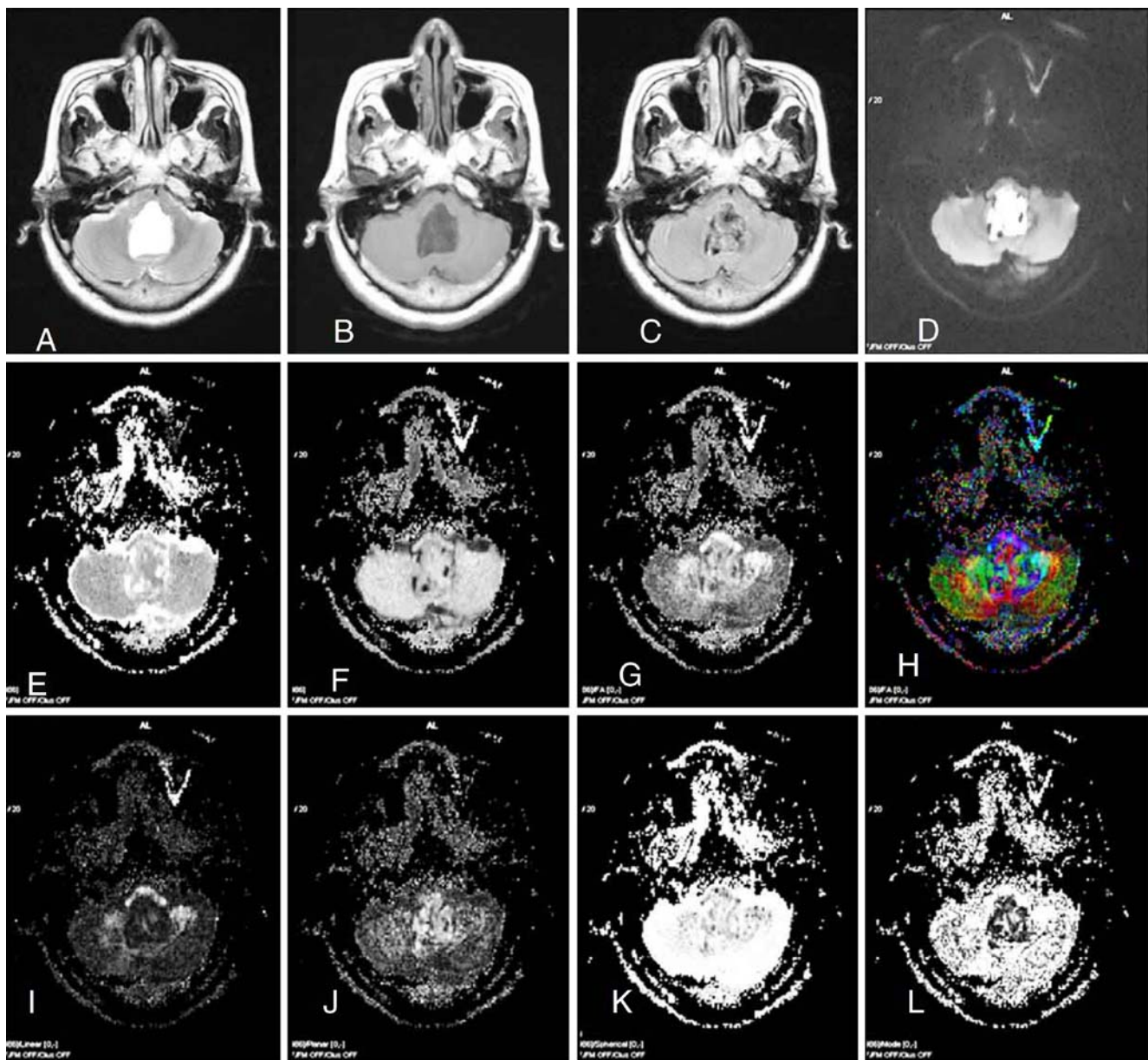
Fig. 2 Case 9: Fourth ventricular epidermoid cyst, which appears hyperintense on T2-weighted image (**A**), hypointense on T1-weighted image (**B**), and heterogeneous on axial FLAIR image (**C**). Diffusion trace image (**D**) shows the lesion to be hyperintense, while on apparent diffusion coefficient map (**E**) and exponential diffusion image (**F**) it appears isointense. FA (**G**) and directionally color-encoded FA (**H**) maps show increased anisotropy, while CS (**K**) map shows a decrease in isotropic diffusion within the tumor. Lesion appears hyperintense on CP (**J**) map and hypointense on diffusion tensor mode (**L**) and CL (**I**) maps suggesting that the increase in FA is due to preferential diffusion occurring along one plane

Results

Table 1 summarizes the DTM derived from the epidermoid cysts and the normal white matter at various locations. D_{av} values obtained from tumor showed that diffusion was facilitated in epidermoid compared to normal white matter, i.e., internal capsule and splenium (mean 0.909 vs 0.737 and 0.774). Exponential diffusion values also confirmed this finding (mean 0.411 vs 0.481 and 0.464). FA values from tumor were high, but not as high as that from normal white matter (mean 0.467 vs 0.789 and 0.831). Mode values were approaching −1 in the lesion, while it was approaching +1 in the white matter (mean −0.921 vs 0.906 and 0.964). CP values (mean 0.551) were higher and CL values (mean 0.035) were lower in the lesion, while CP values (mean 0.253 and 0.179) were lower and CL values (mean 0.558 and 0.643) were higher in the white matter (Figs. 1 and 2). All the patients were operated on and the
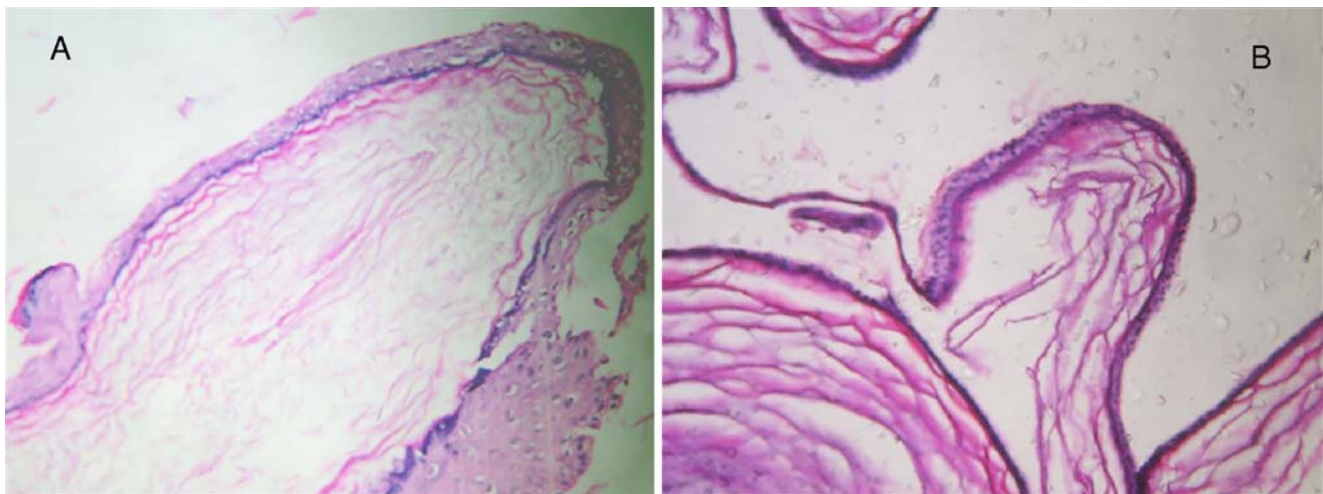
Fig. 3 Photomicrographs of case 9 (**A**) and case 8 (**B**) show epidermoid cysts lined by squamous epithelium. Beneath the epithelial lining, we can see a well-structured parallel-layered arrangement of keratin separated by interstitium. H & E stain, ×200

tumor removed. Histopathological examination in all of them confirmed the diagnosis of epidermoid cysts. On histopathology, parallel layers of keratin flakes were seen separated by interstitium, lying beneath the squamous epithelial lining (Fig. 3).

Discussion

Diffusion-weighted imaging depends on the thermal Brownian motion of water molecules in the tissue [11]. Exponential diffusion and D_{av} values show whether the motion of water molecules is restricted or facilitated. Water mobility may not be equal in all directions (isotropic) but greater in one direction than another (anisotropic), for example, in the white matter. FA is widely used to measure this anisotropy [12, 13]. FA of more than 0.4 generally suggests omnidirectional structural organization [14]:

$$\mu(D_{av}) = \frac{\lambda_1 + \lambda_2 + \lambda_3}{3},$$

$$FA = \sqrt{\frac{3}{2}} \cdot \frac{\sqrt{(\lambda_1 - \mu)^2 + (\lambda_2 - \mu)^2 + (\lambda_3 - \mu)^2}}{\sqrt{\lambda_1^2 + \lambda_2^2 + \lambda_3^2}}.$$

However, tensor shape is intrinsically a trivariate quantity [15, 16]. No two scalar measures (e.g., D_{av} and FA) can account for the degrees of freedom represented by the three eigenvalues. So, to describe the third degree of freedom, we used DTM-like diffusion tensor mode, CL, CP, and CS anisotropy. High FA can be due to either increased linear, planar, or spherical anisotropy which can be differentiated using these DTM [16]. In linear anisotropy,

the predominant direction of diffusion is along a line in the direction of the largest eigenvalue ($\lambda_1 >> \lambda_2$ and λ_3). In the planar anisotropy, the diffusion is restricted to a geometric plane spanned by the two largest eigenvalues ($\lambda_1 \sim \lambda_2 >> \lambda_3$), whereas in the spherical anisotropy, the diffusion is isotropic ($\lambda_1 \sim \lambda_2 \sim \lambda_3$). Diffusion tensor mode helps to differentiate between these three types of anisotropy. These DTM are represented by the following equations:

$$CL = \frac{\lambda_1 - \lambda_2}{\lambda_1 + \lambda_2 + \lambda_3},$$

$$CP = \frac{2(\lambda_2 - \lambda_3)}{\lambda_1 + \lambda_2 + \lambda_3},$$

$$CS = \frac{3\lambda_3}{\lambda_1 + \lambda_2 + \lambda_3},$$

$$CL + CP + CS = 1,$$

$$Mode = \frac{\lambda_1 \lambda_2 \lambda_3}{\left(\sqrt{(\lambda_1 - \mu)^2 + (\lambda_2 - \mu)^2 + (\lambda_3 - \mu)^2}\right)^3}$$

where λ_1, λ_2, and λ_3 represent three eigenvalues of the diffusion ellipsoid. The CL, CP, and CS values measure between 0 and 1 and their sum is unity [17, 18]. Diffusion tensor mode values measures between −1 and +1; it approaches −1 if diffusion is occurring along a geometric plane, approaches +1 if diffusion is occurring along a single direction, and approaches 0 when diffusion is orthotropic or

isotropic [16]. More positive mode and high linear anisotropy indicate preferential diffusion along a single direction; this helps to see the structures which are arranged in linear form, for example, white matter tracts, which facilitate diffusion along one direction. More negative mode and high planar anisotropy indicate preferential diffusion along a geometric plane; they display the structures that are arranged in layers that facilitate diffusion along a particular plane. In this study, we have applied DTI and DTM to study the microstructure of epidermoid cysts.

Epidermoid cysts are derived from the adhesions or inclusions of surface ectoderm into the developing brain [2]. Grossly, they are well-demarcated, encapsulated lesions with whitish capsule and mother-of-pearl sheen, with the interior filled with soft creamy material [19]. Microscopically, they are lined by stratified squamous epithelium mounted on collagenous connective tissue. This epithelium produces keratin, whose progressive production and subsequent desquamation result in formation of concentric lamellae, filling the interior of the cyst, causing its gradual expansion. Cysts also usually contain cholesterol crystals [19]. The radiological features of epidermoid cysts are well described in literature, and they can be diagnosed accurately preoperatively using specific MR sequences [20–22].

In this series, D_{av} from tumor was increased compared to normal white mater, which suggest facilitated diffusion. FA values were also increased, which suggest that diffusion is anisotropic. Furthermore, more negative mode and high planar anisotropy indicated that high FA is due to diffusion occurring along a geometric plane. This is different from white matter, which shows high FA with more positive mode and high linear anisotropy, indicating that high FA is due to diffusion occurring along a single direction. This preferential diffusion along a geometric plane in epidermoid cysts can be explained by looking at their histopathology, which shows well-structured arrangement of the keratin flakes in parallel layers. It could be assumed that these parallel layers of keratin debris limit the diffusion of water in the planes formed between two such layers.

Observed signal change in diffusion-weighted sequence in epidermoid has been attributed to diffusion restriction and/or T2 shine through effect [3–5]. However, this is still controversial. In this study, we clearly see that there is increased T2 relaxation time and increase in D_{av} and FA within these tumors. Probably, the increased extracellular compartment of water between the stacks of keratin causes prolonged T2 relaxation, resulting in bright signal intensity on T2-weighted sequences. Also, the increased T2 relaxation time and increased mean diffusivity suggest that high signal on DWI is due to T2 shine through effect rather than due to restricted diffusion. Increased FA with increased D_{av} can be

explained. Though diffusion is anisotropic and restricted to a geometric plane (more negative mode and high CP), it is high enough in that plane to show increased D_{av}.

Conclusion

This study uses DTI with DTM and shows that FA values are high within the epidermoid cysts, and this high FA is due to increased diffusion along planes formed by layers of keratin as shown by more negative mode and high CP values. High signal intensity of epidermoid cysts seen in diffusion-weighted sequences is possibly due to the T2 shine through effect. Thus, DTM opens a new avenue of opportunities to study the microstructure of epidermoid cysts and can be similarly used for other brain lesions.

References

1. Morrison G, Sobel DF, Kelley WM, Norman D (1984) Intraventricular mass lesions. Radiology 153:435–442
2. Smirniotopoulos JG, Yue NC, Rushing EJ (1993) Cerebellopontine angle masses: radiologic–pathologic correlation. Radiographics 13:1131–1147
3. Bergui M, Zhong J, Bradac GB, Sales S (2001) Diffusion weighted images of intracranial cyst-like lesions. Neuroradiology 43:824–829. doi:10.1007/s002340100595
4. Annet L, Duprez T, Grandin C, Dooms G, Collard A, Cosnard G (2002) Apparent diffusion coefficient measurements within intracranial epidermoid cysts in six patients. Neuroradiology 44:326–328
5. Hakyemeza B, Aksoyb U, Yildizc H, Ergind N (2005) Intracranial epidermoid cysts: diffusion-weighted, FLAIR and conventional MR findings. Eur J Radiol 54:214–220. doi:10.1016/j.ejrad.2004.06.018
6. Sundgren PC, Dong Q, Go'mez-Hassan D, Mukherji SK et al (2004) Diffusion tensor imaging of the brain: review of clinical applications. Neuroradiology 46:339–350. doi:10.1007/s00234-003-1114-x
7. Toh CH, Castillo M, Wong AMC et al (2008) Differentiation between classic and atypical meningiomas with use of diffusion tensor imaging. AJNR Am J Neuroradiol. doi:10.3174/ajnr.A1170
8. Tropine A, Dellani PD, Glaser M et al (2007) Differentiation of fibroblastic meningiomas from other benign subtypes using diffusion tensor imaging. J Magn Reson Imaging 25:703–708. doi:10.1002/jmri.20887
9. Beppu T, Inoue T, Shibata Y, Yamada N et al (2005) Fractional anisotropy value by diffusion tensor magnetic resonance imaging as a predictor of cell density and proliferation activity of glioblastomas. Surg Neurol 63:56–61. doi:10.1016/j.surneu.2004.02.034
10. Goebell E, Fiehler J, Ding XQ et al (2006) Disarrangement of fiber tracts and decline of neuronal density correlate in glioma

patients—a combined diffusion tensor imaging and 1 h-MR spectroscopy study. AJNR Am J Neuroradiol 27:1426–1431

11. Hagmann P, Jonasson L, Maeder P et al (2006) Understanding diffusion MR imaging techniques: from scalar diffusion-weighted imaging to diffusion tensor imaging and beyond. Radiographics 26:S205–S223. doi:10.1148/rg.26si065510

12. Le Bihan D, Mangain JF, Poupon C et al (2001) Diffusion tensor imaging: concepts and applications. J Magn Reson Imaging 46:18–23

13. Thomas B, Sunaert S (2005) Diffusion tensor imaging: technique, clinical and research applications. Riv Neuroradiol 18:419–435

14. Chenevert TL, Sundgren PC, Ross BD (2006) Diffusion imaging: insight to cell status and cytoarchitecture. Neuroimaging Clin N Am 16:619–632. doi:10.1016/j.nic.2006.06.005

15. Bahn MM (1999) Invariant and orthonormal scalar measures derived from magnetic resonance diffusion tensor imaging. J Magn Reson 141:68–77. doi:10.1006/jmre.1999.1875

16. Ennis DB, Kindlmann G (2006) Orthogonal tensor invariants and the analysis of diffusion tensor magnetic resonance images. Magn Reson Med 55:136–146. doi:10.1002/mrm.20741

17. Peled S, Gudbjartsson H, Westin CF, Kikinis R, Jolesz FA (1998) Magnetic resonance imaging shows orientation and asymmetry of white matter fiber tracts. Brain Res 780:27–33. doi:10.1016/S0006-8993(97)00635-5

18. Kumar K, Gupta RK, Nath K et al (2007) Can we differentiate true white matter fibers from pseudofibers inside a brain abscess cavity using geometrical diffusion tensor imaging metrics? NMR Biomed 21(6):581–588. doi:10.1002/nbm.1228

19. Lantos PL, Louis DN, Rosenblum MK, Kleihues P (2002) Tumors of nervous system. In: Graham DI, Lantos PL (eds) Greenfield's neuropathology. vol. II. 7th edn. Arnold, London, pp 964–965

20. Steffy DJ, De Fillip GJ, Spera T, Gabrielson T (1988) MR imaging of primary epidermoid tumors. J Comput Assist Tomogr 12:438–440

21. Kallmes DF, Provenzale JM, Cioft HJ, McClendon RE (1997) Typical and atypical MR imaging features of intracranial epidermoid tumors. AJR Am J Roentgenol 169:883–887

22. Ikushima I, Korogi Y, Hirai T, Sugahara T et al (1997) MR of epidermoids with a variety of pulse sequences. AJNR Am J Neuroradiol 18:1359–1363